

# Improvements to Frank-Wolfe optimization for multi-detector multi-object tracking

R. Henschel<sup>1</sup> L. Leal-Taixé<sup>2</sup> D. Cremers<sup>2</sup> B. Rosenhahn<sup>1</sup>

<sup>1</sup>Leibniz University Hannover <sup>2</sup>Technical University Munich

## Abstract

This paper proposes a novel formulation for the multi-object tracking-by-detection paradigm for two (or more) input detectors. Using full-body and heads detections, the fusion helps to recover heavily occluded persons and to reduce false positives. The assignment of the two input features to a person and the extraction of the trajectories is commonly solved from one binary quadratic program (BQP). Due to the computational complexity of the NP-hard QP, we approximate the solution using the Frank-Wolfe algorithm. We propose several improvements to this solver affecting better minimization and shorter computations, compared to off-the-shelf BQP-solvers and the standard Frank-Wolfe algorithm. Evaluation on pedestrian tracking is provided for multiple scenarios, showing improved tracking quality over single input feature trackers and standard QP-solvers. Finally we present the performance of our tracker on the challenging MOT16 benchmark, being comparable to state-of-the-art trackers.

## 1. Introduction

Multiple object tracking, and in particular people tracking, is one of the key problems in Computer Vision with potential impact for many applications such as video surveillance or autonomous driving. A common approach to generate the trajectories of multiple people is *tracking-by-detection*: first a person detector is applied to each individual frame to find the putative locations of people. Then, these hypotheses are linked across frames to form trajectories. By building on the advances in person detection over the last decade, tracking-by-detection has been very successful [41, 47, 65, 30, 31, 16, 63, 14]. But, at the same time, the dependence on detection results, typically bounding boxes, is also a major limitation. A lot of potentially useful information is lost during the non-maxima suppression. A tracker typically does not use direct image data, except in the form of appearance models used to discriminate different people. Recently, a number of approaches

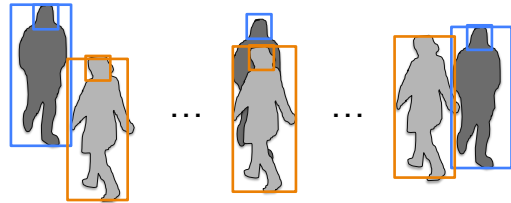


Figure 1. In crowded scenarios occlusions are frequent, with detectors often having many false negatives. By using also *e.g.* head detectors, we are able to recover the trajectory through occlusions.

have proposed to step away from the standard paradigm [46, 26, 13] and instead tackle the tracking problem more directly, using other image features aside from detections, helping especially to recover partly occluded pedestrians missed by the detector.

In this paper, we present a framework to perform multiple object tracking using different input features, in our case, full body and head detections. Our joint formulation treats all features equally, rather than using each feature for a specific purpose. We formulate the feature association as a Binary Quadratic Program (BQP). Conceptually, the solution of the BQP groups all input features belonging to a person, spatially as well as temporally.

A straightforward approach is then to solve an equivalent binary linear program (BLP), using branch&bound. However, due to the high dimensionality of the problem, such BLP is computationally and memory expensive.

By using the Frank-Wolfe algorithm we can solve our non-convex problem in its relaxed form. However, the solution obtained is often not very close to the binary optimal solution. Therefore, we propose two modifications to the Frank-Wolfe algorithm that lead in practice to a much better solution, thus resulting in an improvement of the tracking performance. At the same time, the proposed algorithm is much faster than the standard branch&bound algorithm. We analyze the impact of our modifications on several sequences and demonstrate that the proposed solver delivers better solutions compared to the FW solver, and very close to the optimal solution of the BQP. Finally, an analy-

sis on the effect of the two input feature features shows that the best tracking accuracy is obtained by using both input sources. Improvements can be seen especially in removing false positive full-body detections that are not consistent with the head detections and to recover heavily occluded persons (see Fig. 1 and Fig. 2).

### 1.1. Contributions

To summarize, our contribution is two-fold:

- We present a novel feature coupling formulation for multi-target tracking and demonstrate its improved performance using two types of state-of-the-art features.
- We present several improvements to the standard Frank-Wolfe algorithm, when applied to discrete optimization problems.

### 1.2. Related work

**Optimization in tracking.** Tracking-by-detection has become the standard paradigm for multi-object tracking. It splits the problem into two steps: object detection and data association. In crowded environments, where occlusions are common, even state-of-the-art detectors [20, 23, 54] are prone to false alarms and missed detections. The goal of the data association step is then to fill in the gaps between detections and filter out false positives. In order to do this robustly, it is common to perform data association for all frames and all trajectories simultaneously. This is usually done in discrete space, using Linear Programming [32, 66, 52, 4] or graph-theoretic methods [16, 7, 30], although there are also continuous formulations [47]. Most of these methods can be solved optimally, though some not efficiently, as they require the use of expensive decomposition methods [44, 10]. In contrast, we propose a modification of the FW optimizer that still treats the problem globally and is faster than traditional solvers.

Recently, multiple people tracking has seen improvement by considering data association as a subgraph decomposition problem [65, 16, 62, 63], which implicitly ensures long-term temporal consistency through transitivity constraints while still being based on node to node affinities, keeping the approach computational feasible. In [65] trajectories are created iteratively, computing one best clique corresponding to exactly one person and then removing the corresponding detections from the loop. This concept has been extended in [16] to obtain the trajectories in a global manner, for all persons at the same time. To keep the approach computational feasible, the authors follow a hierarchical approach, connecting heuristically computed initial tracklets via the clique search. Our proposed tracker computes also all trajectories in a global manner, but in contrast to [16], is fast enough to be able to directly optimize on

the detector’s input, thereby avoiding error propagation that might have been introduced during the tracklet creation.

To enforce transitivity in the data association, the work of [16, 62, 63] has to define many cycle/clique constraints in their BLP, making the constraint set huge. In contrast to that, the quadratic formulation proposed in this paper needs only one constraint per cluster. The transitivity is satisfied automatically and implicitly by the quadratic formulation, making especially the Frank-Wolfe iterations with a linear objective very efficient. Furthermore, we adapt the subgraph decomposition to the multi-feature case.

**Frank-Wolfe Algorithm in Computer Vision.** For many problems in Computer Vision, deriving binary solutions using FW has shown great success in terms of quality and reducing the computational costs at the same time [59, 17, 33, 1]. In [33], the localization of similar objects within multiple images/videos is approximated by applying the FW algorithm to a convex function. While it showed good performance, our proposed hierarchical solving scheme can be easily integrated into their formulation, thereby further improving the FW result without high costs. Another application of Frank Wolfe can be found in [59], where object segmentation in videos is tackled. Our modification of the cost function extends their presented non-convex refinement, without the need of a fixed weight that was learned from training data. All these works apply the FW algorithm to a quadratic problem. In that case, the optimal step size for an iterate update during the FW iteration can be computed algebraically and cheap at the same time. We present these computations that go beyond [38, 17, 1], containing all cases that may occur.

**Incorporating different features.** Limiting the input of the tracker to detections has clearly several drawbacks, since much of the information of the image is not taken into account, potentially ignoring semi-occluded objects. In recent literature, several works have started incorporating different image features for the task of multi-target tracking. Few works use supervoxels as input for tracking, obtaining as a byproduct a silhouette of the pedestrian. In [13], supervoxels are labeled according to target identities with greedy propagation, starting from manually initialized segmentation masks. In [46], supervoxel labeling is formulated as CRF inference, where the targets are modeled as volumetric ‘tubes’ through the sequence.

There are several works that use dense point tracks or KLT tracks together with detections to improve tracking performance. In [3], corner features are tracked using KLT to obtain a motion model between detections. The main difference to our tracking paradigm is that the input features are treated differently, not coequally. In [25], multi-target tracking is tackled by clustering dense feature tracks [8] and later extended to [26], where dense point tracklets are combined with detection-based tracklets in a two-step

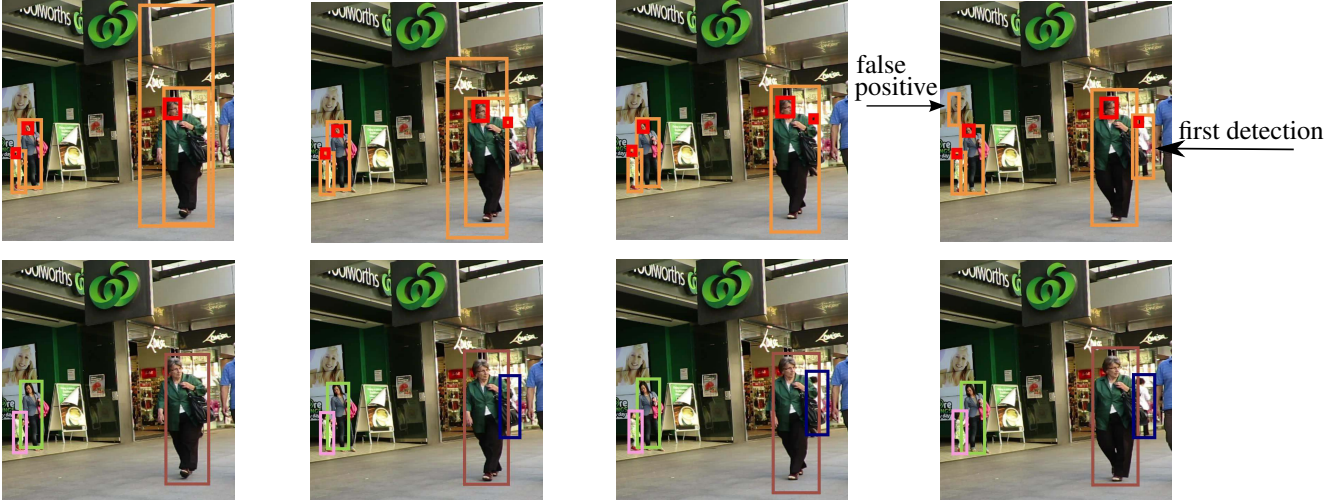


Figure 2. (Top Row.) Input body detections (orange) and head detections (red). The body detector finds the marked person not until the 4th frame. (Bottom row) The result by our tracker. It removes a false positive that has no head detection and recovers the heavily occluded person due to the presence of head detections.

approach.

In contrast, we propose a global optimization formulation to integrate different feature types coequally, so as to take full advantage of the strength of both.

In [12], a quadratic program is proposed to track head and pedestrian detections, modeling non-maxima suppression as well as overlap consistency between features. In contrast to our model, only co-occurrences of active features are considered, while we directly model the grouping of features to different persons, allowing to ensure consistency within each cluster. Also in the extension [59] to motion segmentation using superpixels, the per-person consistency is not considered.

## 2. Multi-target tracking beyond detections

In this section, we describe the data association that couples two (or more) feature types coequally. While other works use each feature type for a certain purpose, *e.g.* detections for localization and optical flow as motion model, our formulation treats all input features equally. This is especially useful in crowded scenarios. Let us imagine the case where a pedestrian is partially occluded. While a full body detector might not localize that pedestrian, a head detector could find the head of the person, even if most parts of the person are occluded. By allowing both types of features to generate trajectories, we are able to increase tracking accuracy. Note that our coupling formulation is general enough to fuse any two (or even more) input features, making the grouping spatial and time consistent.

In this paper, we analyze the impact of coupling full body detections with head detections [61], which are features commonly used in tracking. Evaluations in Sect. 4

show that by using our formulation the tracker benefits most from all feature inputs.

Thereby, the fusion and tracking result is obtained from one binary quadratic optimization problem (BQP). As such problems are NP-hard [57], we rely on finding a good approximation to the solution.

The Frank-Wolfe [27] algorithm is an iterative first-order optimization algorithm especially well suited for quadratic problems with linear constraints, as each iteration step involves solving a computationally efficient linear optimization problem. Since our cost function will be non-convex, Frank-Wolfe delivers only a local optimum. In this paper, we thus focus on improving the Frank-Wolfe solution towards a better optima. We propose to achieve this by: (i) reformulating the cost function and (ii) introducing a hierarchical solving scheme that can easily improve the quality of the solution.

The cost function will be adapted to integrate a regularizer that helps the Frank-Wolfe algorithm to find discrete solution even when solving in the continuous space.

The hierarchical solving scheme gains the improvement by revoking or connecting clusters of the Frank-Wolfe solution, while having the guarantee of operating optimally. The presented approach is not specific to the Frank-Wolfe solver. It can be used in conjunction with any other approximating algorithm. It further allows for local refinement, thereby correcting errors due to the approximation of the initial solver. Experiments in Sect. 4 show that our proposed solver provides good solutions close to the estimated bound, while being considerably faster than the commercial solver Gurobi [29], which uses the branch-and-bound/cut algorithm [39, 49] to find the globally optimal solution.

## 2.1. Joint Data Association

We introduce the notation needed to describe our feature coupling tracking system using a graph-theoretic language. We refer to [19] for readers not familiar with the basics in that field.

The input for our proposed tracker are pairwise disjoint input feature sets  $F_1, \dots, F_d$  that are used to build a vertex-labeled graph  $G$  with vertices  $V = F_1 \cup \dots \cup F_d$ . The edge set  $E := V^{(2)}$  consists of all two-element node sets, so that  $G$  is the complete graph. Since  $G$  is vertex-labeled, we have canonically  $V \simeq \{1, \dots, n\}$ . Furthermore let  $[K] := \{1, \dots, K\}$ .

Now the tracking problem is to find at most  $K$  induced subgraphs in  $G$ . Each subgraph represents the trajectory of a person, consisting of heads and full body detections, thus solving also the feature fusion (see Fig. 3). For nodes  $u, v \in V$  we define unary costs  $c_v \in \mathbb{R}$  and pairwise costs  $q_{u,v} \in \mathbb{R}$ . Thereby,  $c_v$  represents the confidence of a detection and  $q_{u,v}$  reflects temporal or spatial affinities, *i.e.*, compatibility of the head location w.r.t a body detection. We set  $Q_{\text{aff}} = (q_{u,v})_{u,v \in V}$  and  $c_{\text{un}} = (c_v)_{v \in V}$ .

We define a bijection from a given node  $v \in V$  and cluster indexed by  $k \in [K]$  to a component  $x_{i_G(v,k)}$  of a vector  $x \in [0, 1]^{nK}$ . Formally, let  $v \in V$  and  $k \in [K]$ . Then

$$i_G(v, k) = v + n(k - 1) \in [nK] \quad (1)$$

holds the vector position corresponding to node  $v$  in the  $k$ th cluster. In the case of  $x \in \{0, 1\}^{nK}$ , the value  $x_{i_G(v,k)} \in \{0, 1\}$  indicates whether  $v$  belongs to the  $k$ th induced subgraph (or cluster).

To simplify the notation, we shall often omit the subscript  $G$ .

Finally we define an orientation  $D_E \subset V \times V$  on the edge set via  $e = \{v, v'\} \in E$  iff. either  $(v, v') \in D_E$  or  $(v', v) \in D_E$ .

Given the unary and pairwise potentials

$$\text{un}_G(x) := \sum_{\substack{v \in V \\ k \in [K]}} c_v x_{i(v,k)} \quad (2)$$

and

$$\text{pa}_G(x) := \sum_{\substack{(v,v') \in E_A \\ k \in [K]}} q_{v,v'} x_{i(v,k)} x_{i(v',k)}, \quad (3)$$

we define the cost function

$$f_G(x) = \text{un}_G(x) + \text{pa}_G(x). \quad (4)$$

Then our feature fusing tracking problem is to minimize a quadratic program (QP):

$$\min_x f_G(x) \quad (5)$$

subject to:

$$(i) x \in \{0, 1\}^{nK}, \quad (ii) x \in C_G. \quad (6)$$

Thereby the constraint set

$$C_G := \{x \in [0, 1]^{nK} \mid \sum_{k=1}^K x_{i(v,k)} \leq 1, \forall v \in V\} \quad (7)$$

ensures that each input feature is assigned to at most one cluster  $k \in [K]$ , *i.e.* to at most one person. Setting

$$Q = \text{diag}(\underbrace{Q_{\text{aff}}, \dots, Q_{\text{aff}}}_{K \text{ times}}) \in \mathbb{R}^{nK \times nK}, \quad (8)$$

$$c = (\underbrace{c_{\text{un}}^T, \dots, c_{\text{un}}^T}_{K \text{ times}})^T \in \mathbb{R}^{nK}, \quad (9)$$

we obtain  $f_G$  in matrix-vector form, that is

$$f_G(x) = \frac{1}{2} x^T Q x + c^T x. \quad (10)$$

$Q$  is constructed by placing  $K$  copies of the affinity cost matrix  $Q_{\text{aff}}$  at the diagonal. Analogously, we concatenate  $K$  copies of  $c_{\text{un}}$  to obtain  $c$ .

The affinities  $Q_{\text{aff}}$  are obtained from a linear logistic model, since then, problem (5) is equivalent to finding a maximum likely subgraph decomposition in at most  $K$  clusters [62]. Thus for the unary terms we set

$$c_v := \log\left(\frac{1 - \text{conf}(v)}{v}\right) \quad (11)$$

with  $\text{conf}(v)$  denoting the confidence for feature  $v$  (as given by the detector). For the pairwise costs, we learn model parameters  $\theta$  to obtain probabilities

$$p_{u,v} = p(x_{i(u,k)} = 1 \wedge x_{i(v,k)} = 1 \mid \mathbf{f}, \theta), \quad (12)$$

given  $\theta$  and a feature vector  $\mathbf{f}$ , equally defined for all  $k \in [K]$ . Accordingly, the pairwise costs are

$$q_{u,v} := \log\left(\frac{1 - p_{u,v}}{p_{u,v}}\right). \quad (13)$$

In Section 3, we describe the model features  $\mathbf{f}$  used for the classifier.

We note that our tracking problem can be equivalently formulated as a non-proper graph coloring problem (in at most  $K$  colors). Each node is assigned a color  $\{0, 1, \dots, K\}$  where a 0-colored node means that the node is removed in the subgraph decomposition. To each color  $k > 0$  we obtain a corresponding induced subgraph of  $G$  using all nodes of color  $k$ , producing exactly the clusters that that are obtained from the BQP (5).

Detections/features that are temporally too far apart can neither be compared reliably nor meaningfully. Thus, for an

edge  $e = \{v, v'\}$  connecting features of to long temporal distance, the corresponding edge weight is set to  $q_{v,v'} := 0$ , so that the edge becomes irrelevant to the QP minimization (5). Thus, this strategy effectively sparsifies the graph  $G$  and keeps the proposed approach memory and computationally efficient (see Fig. 3).

Finally note that while the approach presented in this paper can benefit from an arbitrary number of input detectors  $d$  with the formulation presented in this section, we discuss an implementation with  $d = 2$ , using full-body and head detection. Applying more than two detectors is thus straightforward. The difference to the implementation presented in this paper lies only in the probabilities/affinities that need to be defined between any types of input features, using the regression presented in Sect. 3.

## 2.2. Frank Wolfe Optimization

Solving the BQP (5) is a challenging task due the fact that it belongs to the NP-hard problems and that our domain space is very high-dimensional. We thus follow a common practice and consider the relaxed problem:

$$\min\{f_G(x) \mid x \in C_G\}. \quad (14)$$

However, even the relaxation is still NP-Hard to solve [51], as  $f_G$  will be non-convex. Thus even for commercial quadratic solvers such as Gurobi [29], minimizing (5) or its relaxation is computationally very expensive.

Consequently, this paper investigates the use of the Frank Wolfe algorithm for the relaxation, and points out ways to further improve its solution. While it is mostly applied to convex functions, we note that it may also be used in the non-convex setting, thereby obtaining a feasible local optimum [36]. We present pseudo-code of the Frank-Wolfe algorithm in Alg. 1 and its evaluation, as a baseline, in Sec. 4.

In Ln. 5 of Alg. 1, the linear approximation of  $f_G$  is minimized, whose solution is  $s^\rho$ . The next iterate  $x^{\rho+1}$  is the minimizing vector between  $x^\rho$  and  $s^\rho$  (Ln. 11). For the optimal step size  $\gamma_\rho$  in Ln. 6, we present an efficient algebraic description in Sect. 2.2.1. The algorithm is stopped in case of a small duality gap  $g_\rho$  or a maximal number of iterations.

Thereby, the best solution  $x_{\min}$  is retrieved either from an iterate  $x^\rho$  (Ln. 12-15), or, (Ln. 7-10) from  $s^\rho$ , as the constraint matrix corresponding to our chosen constraint set  $C_G$  is totally unimodular. Therefore, Ln. 5 delivers a pool of feasible discrete solutions, similar to [33]. Finally, given an iterate  $x^\rho$ , we round in Ln. 12 via

$$\bar{x} = \arg \min_{x \in \{0,1\}^{n_K} \cap C_G} \|x^\rho - x\|_2^2. \quad (15)$$

In order to improve the convergence rate, we use the Frank-Wolfe Variant with Away-Steps that considers a second possible direction the  $\rho$ -th iterate can move to (which is

---

### Algorithm 1: Frank Wolfe Algorithm

---

**Data:** Function  $f$ , feasible point  $x^0$ , IMAX

**Result:** Solution vector  $x_{\min}$

```

1  $c_{\min} = \infty$ ;
2  $\rho = -1$ ;
3 repeat
4    $\rho = \rho + 1$ ;
5    $s^\rho = \arg \min\{s \nabla f_G(x^\rho) \mid s \in C\}$ ;
6    $\gamma_\rho = \arg \min_{\gamma \in [0,1]} f_G(x^\rho + \gamma u^\rho)$ ;
7   if  $f_G(s^\rho) < c_{\min}$  then
8      $c_{\min} = f_G(s^\rho)$ ;
9      $x_{\min} = s^\rho$ ;
10  end
11   $x^{\rho+1} = x^\rho + \gamma_\rho(s^\rho - x^\rho)$ ;
12  if  $f_G(\text{ROUND}(x^{\rho+1})) < c_{\min}$  then
13     $c_{\min} = f_G(x^{\rho+1})$ ;
14     $x_{\min} = x^{\rho+1}$ ;
15  end
16 until  $g_\rho := (u^\rho)^\top (-\nabla f_G(x^{\rho+1})) < \epsilon \vee \text{iter} > \text{IMAX}$ ;

```

---

away from an atom). We refer the interested reader to [37] for further details.

#### 2.2.1 Computing the optimal step size $\gamma$

The step size  $\gamma$  in Ln. 6 can be computed via line search [5]. However, we present an algebraic computation, being faster and still optimal, as  $f_G$  is a quadratic function.

To this end, define  $\Omega(\gamma) := f_G(x^\rho + \gamma s^\rho)$ . Then

$$\begin{aligned} \Omega'(\gamma) &= 0 \Leftrightarrow \gamma = \frac{-\nabla f_G(x^\rho)^\top s^\rho}{(s^\rho)^\top Q s^\rho}, \\ \Omega''(\gamma) &= 2(s^\rho)^\top Q s^\rho. \end{aligned}$$

Now let  $\bar{\gamma} \in \mathbb{R}$  be the root of  $\Omega'$  and  $\delta = \Omega''(\bar{\gamma})$ . Since  $\Omega(\gamma)$  is quadratic, we obtain the optimal  $\gamma \in [0, 1]$  of Ln. 6 via

$$\gamma = \begin{cases} \bar{\gamma} & \text{if } \delta > 0, \bar{\gamma} \in [0, 1] \\ 0 & \text{if } (\delta > 0, \bar{\gamma} \leq 0) \text{ or } (\delta < 0, \bar{\gamma} \geq 1) \\ 1 & \text{if } (\delta > 0 \text{ and } \bar{\gamma} \geq 1) \text{ or } (\delta < 0 \text{ and } \bar{\gamma} \leq 0) \\ \arg \min_{\gamma \in \{0,1\}} (\Omega(\gamma)) & \text{if } \delta < 0 \text{ and } \bar{\gamma} \in (0, 1). \end{cases}$$

A line search is required only if  $\delta = 0$ , making Ln. 6 very efficient. In contrast to previous works [38, 17], our solution to Ln. 6 contains all cases that may occur.

#### 2.2.2 Reduction of the input dimension

The structure of Alg. 1 allows to reduce the input dimension significantly: Instead of directly plugging in 10 into a



Figure 3. (Top row) Illustrative example of full-body detections and head detections in the MOT16-11 sequence. For simplicity only detections regarding the two selected persons at the right side are shown. (Bottom row) Any input detection is assigned to a node. Any two nodes are linked via an graph edge  $e \in E$ . Edges connecting nodes that are temporally too far apart are assigned a zero edge-weight. We therefore do not draw those edges, as they are irrelevant to the QP minimization. Edges of the same color indicate clustered detections, whereas dashed edges are drawn in cases where the nodes do not belong to the same cluster. Equivalently, computing the induced subgraphs from all nodes having the same color produces the two clusters.

standard QP-solver, we only need to store the costs matrix  $Q_{\text{aff}}$  and vector  $c_{\text{un}}$ . Then, all steps of Alg. 1 can be processed using these matrices, thus being memory efficient. For example, let

$$u^{\rho,k} = \begin{pmatrix} x_{i(1,k)}^{\rho} & \cdots & x_{i(n,k)}^{\rho} \end{pmatrix} \in \mathbb{R}^{n \times 1}, \quad (16)$$

for  $k \in [K]$ . Then, we obtain

$$Qx^{\rho} = \begin{pmatrix} Q_{\text{aff}}u^{\rho,1} & \cdots & Q_{\text{aff}}u^{\rho,K} \end{pmatrix}^{\top} \in \mathbb{R}^{nK \times 1}. \quad (17)$$

Similarly all terms containing  $Q$  or  $c$  can be replaced using  $Q_{\text{aff}}$  and  $c_{\text{un}}$ .

### 2.2.3 Rounding of the solution

In order to obtain a discrete solution from the iterates  $x^{\rho}$  in Ln. 12, we follow the standard approach and round using the euclidean distance:

$$\bar{x} = \arg \min_{x \in \{0,1\}^{nK} \cap C_G} \|x^{\rho} - x\|_2^2. \quad (18)$$

Note that the BQP (18) can be reformulated as a binary linear problem. To this end, let  $\mathcal{C} := \{0,1\}^{nK} \cap C_G$ . Then,

$$\bar{x} = \arg \min_{x \in \mathcal{C}} \|x^{\rho} - x\|_2^2 = \arg \min_{x \in \mathcal{C}} \sum_{i=1}^{nK} (x_i^{\rho} - x_i)^2 \quad (19)$$

$$= \arg \min_{x \in \mathcal{C}} \sum_{i=1}^{nK} -2x_i^{\rho}x_i + x_i^2 \quad (20)$$

$$= \arg \min_{x \in \mathcal{C}} \sum_{i=1}^{nK} -2x_i^{\rho}x_i + x_i, \quad (21)$$

where (20)  $\iff$  (21) holds since  $x$  is a binary vector and thus  $x_i^2 = x_i$  for all  $i$ . Now since the constraint matrix corresponding to  $C_G$  is totally unimodular, we can efficiently solve the relaxation and obtain the exact solution of (18).

### 2.3. Regularization

Our next proposed improvement to the FW algorithm is to add a regularization term to  $f_G$ . One strategy is to enforce convexity [12, 33, 9, 6]. However, we observed that a convex objective function resulted in the degenerated constant  $(\frac{1}{K+1})$  vector as FW output, as also noted in [59]. Driven by that observation, our aim is to transform  $f$  to a non-convex function. For  $u \in \mathbb{R}_{\geq 0}$ , we set

$$f_u(x) = x^{\top}[Q + u\mathbf{I}_{nK}]x + c^{\top}x - u\mathbf{1}^{\top}x, \quad (22)$$

where  $\mathbf{I}_{nK}$  and  $\mathbf{1}$  denote the diagonal matrix and the constant 1 vector, respectively. Then for  $x \in [0, 1]^{nK}$ ,

$$f_u(x) = f_G(x) + u \sum_j (x_j^2 - x_j) \leq f_G(x) \quad (23)$$

and for  $x \in \{0, 1\}^{nK}$ , we have  $f_u(x) = f_G(x)$ . Intuitively,  $f_u$  pushes FW towards binary solutions, as  $(x_j^2 - x_j)$  is minimal at 0 and 1.

Replacing each diagonal entry of  $Q$  with the absolute sum of each row makes  $Q$  positive semi-definite and the objective function convex. Let  $\omega$  be the maximal absolute row sum value. We then set  $u_0 = \sqrt{\omega}$  and  $u_i = \frac{1}{2^i} u_0$ . Starting with  $u = u_0$ , we solve the relaxation of (5), using  $f_u$ . If the convergence was obtained in too few steps (which we set to 10), we set  $u = u_{i+1}$  and solve it again. Otherwise, we keep the solution. We observed that this strategy finds in nearly all cases a good solution in at most two  $u$  iterations. In Sect. 4, we demonstrate the impact of using the modified cost function, with the solver we call  $FW + u$ .

## 2.4. Hierarchical solving scheme

In order to enhance the result of  $FW + u$ , we propose a new hierarchical solving scheme that gains its improvement by removing, correcting and connecting clusters, while still optimizing the BQP defined in Eq. (5). The algorithm is presented in Alg. 2.

---

### Algorithm 2: Hierarchical solving scheme

---

**Data:** Graph decomp.  $x_G$  into  $k$  clusters, graph  $G$

**Result:** Solution vector  $x_{G-\text{opt}}$

```

1  $x_{G-\text{opt}} = x_G$ ;
2 repeat
3    $\text{bestValue} = f_G(x_G)$ ;
4    $x_{G-\text{opt}} = x_G$ ;
5    $x_{G-\text{locR}} = \text{localRefinement}(x_G)$ ;
6    $\underline{G} = \text{GraphContract}(x_{G-\text{locR}})$ ;
7    $x_{\underline{G}} = \text{solve/approx QP (5) on } \underline{G}$ ;
8    $x_G = \text{GraphExpand}(x_{\underline{G}})$ ;
9 until  $f_G(x_G) \geq \text{bestValue}$ ;
```

---

Let  $\mathcal{D}(G, K)$  be the set of all subgraph decompositions of  $G$  in at most  $K$  components.

A vector  $x^* \in C_G \cap \{0, 1\}^{nK}$  describes a decomposition  $\mathcal{D} \in \mathcal{D}(G, K)$  of  $G$  (see Fig. 4). Defining each cluster  $\mathcal{D} \in \mathcal{D}$  as a node  $v_{\mathcal{D}} := \mathcal{D}$ ,  $G$  is contracted into a graph  $\underline{G}$ , which we call *GraphContract* in Alg. 2 (purple circles in Fig. 4). Having  $k$  connected components  $\mathcal{D}_1, \dots, \mathcal{D}_k$  we define the new graph  $\underline{G} = (\underline{V}, \underline{E})$  with  $\underline{V} = \{v_{\mathcal{D}_1}, \dots, v_{\mathcal{D}_k}\}$  and  $\underline{E} = \underline{V}^{(2)}$ . In order to optimize on Eq. (5), we define the unary costs

$$c_{v_{\mathcal{D}}} := \sum_{v \in V(\mathcal{D})} c_v + \frac{1}{2} \sum_{v, v' \in V(\mathcal{D})} q_{v, v'} \quad (24)$$

and pairwise costs

$$q_{v_{\mathcal{D}}, v_{\mathcal{D}'}} := \sum_{v \in V(\mathcal{D}), v' \in V(\mathcal{D}')} q_{v, v'}. \quad (25)$$

If  $I_{\underline{G}} \in \{0, 1\}^{k^2} \cap C_{\underline{G}}$  is the vector grouping each node  $v_{\mathcal{D}} \in V(\underline{G})$  as a single component, we have

$$f_G(x^*) = f_{\underline{G}}(I_{\underline{G}}). \quad (26)$$

Therefore, solving (5) with  $\underline{G}$  results in a solution  $\hat{x}_{\underline{G}} \in \{0, 1\}^{k^2} \cap C_{\underline{G}}$  with

$$f_{\underline{G}}(\hat{x}_{\underline{G}}) \leq f_{\underline{G}}(I_{\underline{G}}) = f_G(x^*). \quad (27)$$

Finally, we transform  $\hat{x}_{\underline{G}}$  into a vector  $\hat{x} \in \{0, 1\}^{nK} \cap C_G$  such that  $f_{\underline{G}}(\hat{x}_{\underline{G}}) = f_G(\hat{x})$ , by expanding  $\underline{G}$  (*GraphExpand* in Alg. 2, see also Fig. 4) to the original graph  $G$ , thereby maintaining the nodes and its links as given by the solution  $\hat{x}_{\underline{G}}$ .

Note that we can apply a local refinement strategy (*localRefinement* in Alg. 2, see also Fig. 4), correcting obvious errors that may have been introduced due to the rounding or local optimality. To this end, we separate all nodes with positive affinity costs to its connected component as a singleton cluster, as well as nodes that have been rejected by the FW solution, and postpone the decision about their belonging to the next iteration of Alg. 2. Furthermore Ln. 6 in Alg. 2 reduces the dimensionality dramatically, as there are  $k$  nodes to be clustered to at most  $k$  induced subgraphs. In particular, we solve (5) on  $\underline{G}$  quickly to optimality using Gurobi [29]. This makes postponing of unclear decisions reasonable, as we have the guarantee of an optimal solution. Such a strategy shows similarities to [30], where tree tracklets implicitly signal ambiguous connections. Thus, they solve the linkage of the resulting tracklets in a later iteration once enough information become available.

Note that if the node number is still huge to be solved using an optimal discrete solver, the Frank-Wolfe algorithm can be alternatively applied, approximating the solution.

We demonstrate the effect the hierarchical solving scheme ( $FW + u + h$ ) in Sect. 4.

## 3. Regression training

For our tracking system, we consider two input features: (i) full body and (ii) head detections (see also Fig. 1 and Fig. 2). Note that features such as superpixels [11] or point trajectories [50] could also be used within our framework, nonetheless we choose the aforementioned features due to their popularity in recent years in the field of tracking. As explained in Sect. 2.1, we train a linear regression model for the spatial and temporal affinities, using the software [22]. The affinities will be mapped to the costs that form our optimization problem, according to Eq. (13).

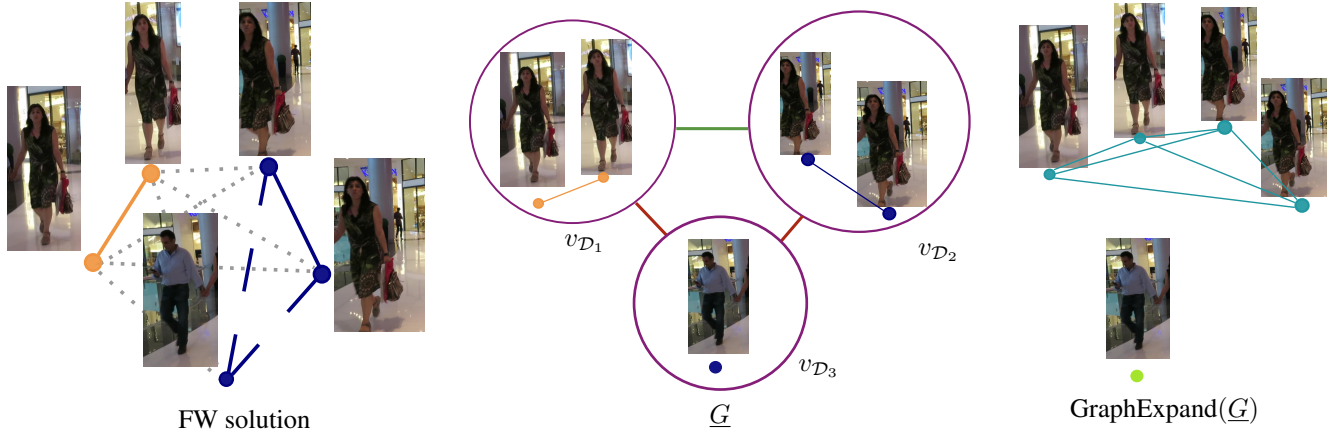


Figure 4. (Left.) A solution  $x^*$  of Alg. 1. Dotted edges indicate removed links. Nodes connected by edges of the same color are grouped, resulting in two clusters. Dashed edges indicate wrong connections. (Middle.) Each cluster is replaced by a new node (purple circles). Wrongly connected nodes (the men’s node) are separated in the *localRefinement* step. On  $\underline{G}$ , problem (5) is solved w.r.t. the purple circles as nodes, and the edges between them as possible links. The green line shows the selected edge. (Right.) The *GraphExpand* operation produces the corresponding decomposition as shown on the right side.

**Head detections.** To obtain accurate head detections, we employ [61] based on Convolutional Neural Networks and fine-tune it on the MOT16 training set [45].

**Full body detections.** We use the body detections [24] as provided by the MOT16 challenge [45].

**Relative positioning.** In order to obtain meaningful distances between points of differently sized boxes, we need a normalization. To this end given a  $2d$ -point  $p$  and a bounding box  $b$ , we use the lower left and the upper corners of  $b$  to obtain the barycentric coordinates  $bary(p, b) = (\kappa_1, \lambda_1, \mu_1)$  of  $p$  w.r.t.  $b$  (see Fig. 5). Finally, we fix a rectangle  $r$  and map  $bary(p, b)$  to that box using the corners of  $r$ . Then, distance measurements are casted to  $r$ , using euclidean norm.

**Spatial affinities.** We introduce two affinities that set the position of the head in relation to the detection box. Their definition is easily generalized to fuse other possible features.

First, we mirror a head detection to the left half side of a bounding box, making the position robust against different orientations of the person. From the MOT16 training data we learn the expected relative position of a head. Then, we compute the distance  $\|p_{obs} - p_{exp}\|_2$  between the observed and expected position in the fixed rectangle  $r$ . In addition we compare the angle difference to the expected position, with the anchor at the box’s center (see Fig. 5). We set the spatial affinity between features of the same type to a constant high value  $c_{high}$ .

**Temporal affinities.** We employ DeepMatching [64] (DM) in order to define temporal affinities between any two input features, due to their superior stability for temporal associations than spatio-temporal affinities [63]. Comparing two

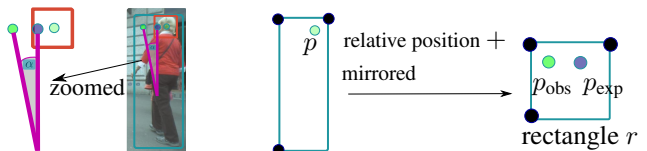


Figure 5. Angle and distance between the expected (blue node) and the observed (mirrored) head position (green node). Barycentric coordinates are computed w.r.t. black corners.

heads or two full-body detections, we divide the number of common DM points in two features by the minimal, maximal and mean number of DM point in the two features, as in [63]. Head detections are significantly smaller than full body detections. Therefore, the temporal head to full body affinity has to be slightly adapted to that case: Instead of the three aforementioned features, we divide the number of DM points in the full-body detection by the number of DM points in the head detection. Furthermore we learn from the training set the expected ratio  $r_{trained}^w$  and  $r_{trained}^h$  between a head and body detection, w.r.t. width and height, respectively. Then we obtain features  $\|r_{trained}^w - r_{current}^w\|_2$  and  $\|r_{trained}^h - r_{current}^h\|_2$ , for the observed ratios  $r_{current}^w$  and  $r_{current}^h$  w.r.t. width and height, respectively.

## 4. Experimental results

In this section we provide details about our implementation of the proposed tracking system. In addition to that we analyze first the gain both in speed as well as in tracking performance of our proposed modifications to the Frank Wolfe algorithm. Next we present an analysis of the tracking performance with several input features on the training se-

quences of the challenging MOTChallenge MOT16 benchmark [45]. This benchmark consists of 7 sequences for training and 7 for testing, with footage of crowded scenes. In the last experiment, we show our performance on the test set of the benchmark where we achieve performance close to state-of-the-art methods.

#### 4.1. Implementation details

We discuss certain details of the implementation regarding the training as well as the creation of the data association graph.

For the head detector [61], we observe the best performance, when it is trained separately for high-definition and low-definition videos, respectively. Therefore, we train the head detector on all high-definition videos of the MOT16 train set, when applied to HD test sequences of MOT16. For the SD sequences, we use the sequence ETH-Bahnhof, ETH-Sunnyday, ETH-Pedcross2, TUD-Campus, TUD-Stadtmitte from the MOT15 train set [42] as well as the MOT16-05 sequence from the MOT16 train set. We manually create ground-truth head detections for all mentioned train sequences and fine-tune the head detector using 55.000 iterations. In cases where we evaluate on the training set in the subsequent experiments, we train for each video the head detector on the remaining other training sequences. Similarly we train the logistic regressors of Sect. 3 using the MOT16 train set. In experiments where we evaluate on a train sequences, we use a regressor that has been trained on all MOT16 train sequences except the one that is being evaluated.

Two nodes of the graph  $G$  defined in Sect.2.1 that are temporally to far apart are assigned a zero weight. We set the maximal temporal distance to  $\text{MAXGAP} := 9$  frames, being a good trade-off between efficiency and reliable comparisons. Furthermore, we set the upper bound on the number of clusters to  $K = 70$ . Note however that presetting  $K$  is just a coarse bound. In case that more clusters are needed it is possible to encode more than  $K$  trajectories using these  $K$  clusters: As nodes that are more than  $\text{MAXGAP}$  frames apart have zero link costs, a cluster may include several trajectories that are separable by the  $\text{MAXGAP}$  frame threshold, without producing wrong results or violating the constraints. For instance a cluster could contain a trajectory  $t_1$  in frame  $1, \dots, 10$ , and another trajectory  $t_2$  in frame  $30, \dots, 50$ . As the temporal distance is bigger than  $\text{MAXGAP}$  frames, we can easily extract  $t_1$  and  $t_2$  from the cluster result. The sequences is processed in batches of maximal size such that they contain no more than 1800 input detections. Using an overlap of 9 frames, we ensure trajectory consistency between the batches.

We stop the Frank-Wolfe iterations of Alg.1, in case that the duality gap is below  $10^{-4}$  or 750 iterations are reached.

Having solved the data association problem using the hi-

Table 1. Values at convergence

Method	Iters	Time	Obj Value	MOTA
$FW$	<b>16</b>	<b>0.7</b>	-3060	14.2
$FW + u$	676	27	-5481	26.8
$FW + u + h$	-	27+0.5	<b>-5925</b>	<b>27.5</b>
Gurobi	-	1000	(-5531)	24.9
Gurobi bound	-	1000	(-5973)	-

erarchical solving scheme, some trajectories will contain only head detections for certain frames. If the trajectory does not contain any full-body detection, we consider the trajectory as a ghost trajectory due to false positive head detections and remove it.

In case that a trajectory contains full body and head detections, we can recover frames in which the trajectory contains only head detections, using the learned classifier of Sect. 3. To this end, given a frame where only the head detection is known, we randomly sample full body detections around the head position and select the best bounding box by taking the one that has the highest probability according to the learned classifier as described in Sect. 3 and keep the newly produced detection in cases that the probability is higher than 75%.

Furthermore, we slightly enlarge head detections in order to include more information of its surrounding like parts of the shoulders and the neck, by enlarging the width and height by factor 1.6.

#### 4.2. Frank-Wolfe optimization

Our first experiment is focused on analyzing the impact of our modifications to the Frank-Wolfe optimization. To this end, we choose a small batch of 40 frames from the MOT16-13 training sequence and perform tracking using detections only. In Table 1 we show the number of iterations performed by the solver until the duality gap is below the defined threshold, the time taken, the final objective value as well as the corresponding Multiple Object Tracking Accuracy (MOTA).

As we can see, our proposed modification  $FW + u + h$  improves the objective value considerably with respect to the standard Frank-Wolfe  $FW$ . This naturally translates to almost double MOTA accuracy, 14.2% vs 27.5%. Note also that the objective value comes very close to the bound given by the commercial solver Gurobi [29], which uses the branch-and-bound algorithm to optimize. Furthermore, Gurobi is still far away from the bound after 1000 seconds, while we obtain a much better energy after only 27.5 seconds.

The energy evolution of the different solvers is plotted in Figure 6. Here we clearly see where  $FW$  stops (red line), how our modification  $FW + u$  improves the energy by a large margin (blue line), and how finally  $FW + u + h$  (yel-

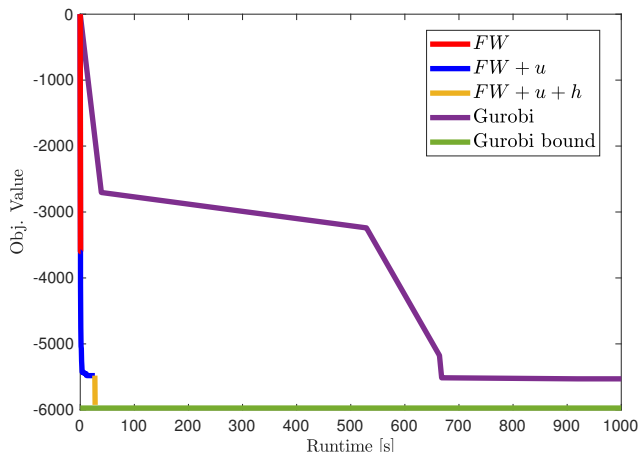


Figure 6. Minimization performance of each BQP solver and the bound as given by Gurobi for each moment.

low line) comes even closer to the bound (green line). On the other hand, Gurobi (purple line) has a much slower convergence.

### 4.3. Tracking with different features

We analyze how our tracking system benefits from two input features. To this end, we apply our tracker to all MOT16 training sequences and report the evaluation in Tab. 2, with full-body detections only (*Body*) against body and head detections (*Body+Heads*). Using the two input features, we observed a significant improvement in almost all relevant tracking metrics, justifying our tracking formulation. Therefore, the MOTA score increases by nearly 5%. Due to the coupling of accurate head detections with body-detections coequally, the number of false positive is reduced by more than 48 % of the initial errors.

Table 2. Feature evaluation on MOT16 training sequences.

	$FW + u + h$				
Feature	MOTA	MT	ML	FP	IDs
Body	31.8	75	231	13747	439
Body+Heads	<b>36.5</b>	<b>86</b>	<b>219</b>	<b>6620</b>	<b>428</b>

### 4.4. Comparison on MOT16 test

Finally, we evaluate the tracking performance of *Body+Heads* on the *MOT16* benchmark and provide the results in Tab. 3, as shown on the website. We are one of the best performing published algorithms in terms of tracking accuracy. Due to the input feature coupling, we have the lowest ML score within all trackers of the *MOT16* Challenge. The low ML score (mostly lost) demonstrates that we can recover more trajectories than any other tracker.

## 4.5. Visual Results

We provide further visual results in Fig. 7. It shows the trajectory results of the proposed system along with the input detections. It shows that we can recover persons that are heavily occluded, as they are still detected by the head detector, resulting in stable long term trajectories. In particular due to the presence of the head position, we are able to recover full-body detections without drifts as they appear when using methods such as linear interpolation.

## 5. Conclusion

We presented a global formulation for the integration of full-body and head detections for multi-target tracking. The problem is cast into a quadratic program, which is solved efficiently via the Frank-Wolfe algorithm. We improved the solver in two ways; (i) regarding time by providing complete and efficient computation of the optimal step size and (ii) regarding minimization by a reformulation of the objective function, resulting in better discrete solutions. Finally we showed that our hierarchical solving scheme improves a feasible solution, often close to optimality and yet is easy to integrate and fast.

The feature coupling delivered superior results when compared to single input features, thus proving the benefits of our formulation. The overall performance on a tracking benchmark showed competitive results compared to state-of-the-art trackers.

## References

- [1] S. M. Assari, H. Idrees, and M. Shah. Re-identification of humans in crowds using personal, social and environmental constraints. *arXiv preprint arXiv:1612.02155*, 2016.
- [2] Y. Ban, S. Ba, X. Alameda-Pineda, and R. Horaud. Tracking multiple persons based on a variational bayesian model. In *ECCV Workshops - Benchmarking Multi-Target Tracking*, 2016.

Table 3. The *MOT16* leaderboard. Performance of several trackers according to different metrics.

Method	MOTA $\uparrow$	MOTP $\uparrow$	MT $\uparrow$	ML $\downarrow$	FP $\downarrow$	FN $\downarrow$	ID $\downarrow$	FM $\downarrow$
NOMT [15]	46.4	76.6	18.3	41.4	9753	87565	359	504
JMC [63]	46.3	75.7	15.5	39.7	6373	90914	657	1114
<b>Ours</b>	44.8	74.1	16.9	37.2	11082	88452	1044	2563
MDPNN16 [56]	43.8	75.5	12.4	40.7	3501	98193	723	2036
oICF [34]	43.2	74.3	11.3	48.5	6651	96515	381	1404
MHT-DAM [35]	42.9	76.6	13.6	46.9	5668	97919	499	659
LINF1 [21]	41.0	74.8	11.6	51.3	7896	99224	430	963
EAMTT_pub [58]	38.8	75.1	7.9	49.1	8114	102452	965	1657
OVBT [2]	38.4	75.4	7.5	47.3	11517	99463	1321	2140
LTTC-CRF [40]	37.6	75.9	9.6	55.2	11969	101343	481	1012
LP2D [43]	35.7	75.8	8.7	50.7	5084	111163	915	1264
TBD [28]	33.7	76.5	7.2	54.2	5804	112587	2418	2252
CEM [48]	33.2	75.8	7.8	54.4	6837	114322	642	731
DP_NMS [53]	32.2	76.4	5.4	62.1	1123	121579	972	944
GMPHD_HDA [60]	30.5	75.4	4.6	59.7	5169	120970	539	731
SMOT [18]	29.7	75.2	5.3	47.7	17426	107552	3108	4483
JPDA_m [55]	26.2	76.3	4.1	67.5	3689	130549	365	638

- [3] B. Benfold and I. Reid. Stable multi-target tracking in real-time surveillance video. In *CVPR*, 2011.
- [4] J. Berclaz, F. Fleuret, E. Türetken, and P. Fua. Multiple object tracking using k-shortest paths optimization. *TPAMI*, 2011.
- [5] D. P. Bertsekas. *Nonlinear programming*. Athena scientific Belmont, 1999.
- [6] A. Billionnet, S. Elloumi, and A. Lambert. Extending the qcr method to general mixed-integer programs. *Mathematical programming*, 131(1):381–401, 2012.
- [7] W. Brendel, M. Amer, and S. Todorovic. Multiobject tracking as maximum weight independent set. In *CVPR*, 2011.
- [8] T. Brox and J. Malik. Object segmentation by long term analysis of point trajectories. In *ECCV*, 2010.
- [9] S. Burer and A. N. Letchford. Non-convex mixed-integer nonlinear programming: A survey. *Surveys in Operations Research and Management Science*, 17(2):97–106, 2012.
- [10] A. Butt and R. Collins. Multi-target tracking by lagrangian relaxation to min-cost network flow. In *CVPR*, 2013.
- [11] J. Chang, D. Wei, and J. W. Fisher. A video representation using temporal superpixels. In *Proceedings of the IEEE Conference on Computer Vision and Pattern Recognition*, pages 2051–2058, 2013.
- [12] V. Chari, S. Lacoste-Julien, I. Laptev, and J. Sivic. On pairwise costs for network flow multi-object tracking. In *CVPR*, 2015.
- [13] S. Chen, A. Fern, and S. Todorovic. Multi-object tracking via constrained sequential labeling. In *CVPR*, 2014.
- [14] W. Choi. Near-online multi-target tracking with aggregated local flow descriptor. In *ICCV*, 2015.
- [15] W. Choi. Near-online multi-target tracking with aggregated local flow descriptor. In *ICCV*, 2015.
- [16] A. Dehghan, S. Assari, and M. Shah. Gmmcp-tracker: Globally optimal generalized maximum multi clique problem for multiple object tracking. In *CVPR*, 2015.
- [17] A. Dehghan and M. Shah. Binary Quadratic Programing for Online Tracking of Hundreds of People in Extremely Crowded Scenes. *arXiv preprint arXiv:1603.09240*, 2016.
- [18] C. Dicle, M. Sznaiar, and O. Camps. The way they move: Tracking multiple targets with similar appearance. In *ICCV*, 2013.
- [19] R. Diestel. *Graph theory*. Springer, 2000.
- [20] P. Dollár, R. Appel, S. Belongie, and P. Perona. Fast feature pyramids for object detection. *TPAMI*, 2014.
- [21] L. Fagot-Bouquet, R. Audigier, Y. Dhome, and F. Lerasle. Improving multi-frame data association with sparse representations for robust near-online multi-object tracking. In *ECCV*, 2016.
- [22] R.-E. Fan, K.-W. Chang, C.-J. Hsieh, X.-R. Wang, and C.-J. Lin. LIBLINEAR: A library for large linear classification. *JMLR*, 9, 2008.
- [23] P. Felzenszwalb, R. Girshick, D. McAllester, and D. Ramanan. Object detection with discriminatively trained part based models. *TPAMI*, 2010.
- [24] P. F. Felzenszwalb, R. B. Girshick, D. McAllester, and D. Ramanan. Object detection with discriminatively trained part-based models. *IEEE transactions on pattern analysis and machine intelligence*, 32(9):1627–1645, 2010.
- [25] K. Fragkiadaki and J. Shi. Detection free tracking: Exploiting motion and topology for segmenting and tracking under entanglement. In *CVPR*, 2011.
- [26] K. Fragkiadaki, W. Zhang, G. Zhang, and J. Shi. Two-granularity tracking: mediating trajectory and detections graphs for tracking under occlusions. In *ECCV*, 2012.
- [27] M. Frank and P. Wolfe. An algorithm for quadratic programming. *Naval Research Logistics Quarterly*, 1956.
- [28] A. Geiger, M. Lauer, C. Wojek, C. Stiller, and R. Urtasun. 3d traffic scene understanding from movable platforms. *PAMI*, 2014.
- [29] I. Gurobi Optimization. *Gurobi Optimizer Reference Manual*. 2015.
- [30] R. Henschel, L. Laura Leal-Taixé, and B. Rosenhahn. Efficient multiple people tracking using minimum cost arborescences. In *GCPR*, 2014.
- [31] R. Henschel, L. Leal-Taixé, and B. Rosenhahn. Solving multiple people tracking in a minimum cost arborescence. In *Winter Conference on Applications of Computer Vision Workshops (WACVW)*, 2015.
- [32] H. Jiang, S. Fels, and J. Little. A linear programming approach for multiple object tracking. In *CVPR*, 2007.
- [33] A. Joulin, K. Tang, and F. F. Li. Efficient image and video co-localization with frank-wolfe algorithm. In *ECCV*, pages 253–268. Springer, 2014.
- [34] H. Kieritz, S. Becker, W. Hübner, and M. Arens. Online multi-person tracking using integral channel features. In *AVSS*, 2016.
- [35] C. Kim, F. Li, A. Ciptadi, and J. M. Rehg. Multiple hypothesis tracking revisited: Blending in modern appearance model. In *ICCV*, 2015.
- [36] S. Lacoste-Julien. Convergence rate of frank-wolfe for non-convex objectives. *arXiv preprint arXiv:1607.00345*, 2016.
- [37] S. Lacoste-Julien and M. Jaggi. On the global linear convergence of frank-wolfe optimization variants. *NIPS*, 2015.
- [38] S. Lacoste-Julien, M. Jaggi, M. Schmidt, and P. Pletscher. Block-Coordinate Frank-Wolfe Optimization for Structural SVMs. In *ICML*, 2013.
- [39] A. H. Land and A. G. Doig. An automatic method of solving discrete programming problems. *Econometrica: Journal of the Econometric Society*, 1960.
- [40] N. Le, A. Heili, and M. Odobez. Long-term time-sensitive costs for crf-based tracking by detection. In *ECCV Workshops - Benchmarking Multi-Target Tracking*, 2016.
- [41] L. Leal-Taixé, M. Fenzi, K. A., R. B., and S. Savarese. Learning an image-based motion context for multiple people tracking. In *CVPR*, 2014.
- [42] L. Leal-Taixé, A. Milan, S. Roth, K. Schindler, and I. Reid. Motchallenge: A benchmark for multi-target tracking. *arXiv*, 2015.
- [43] L. Leal-Taixé, G. Pons-Moll, and B. Rosenhahn. Everybody needs somebody: Modeling social and grouping behavior on a linear programming multiple people tracker. *ICCV. 1st Workshop on Modeling, Simulation and Visual Analysis of Large Crowds*, 2011.
- [44] L. Leal-Taixé, G. Pons-Moll, and B. Rosenhahn. Branch-and-price global optimization for multi-view multi-object tracking. In *CVPR*, 2012.

- [45] A. Milan, L. Leal-Taixé, I. Reid, S. Roth, and K. Schindler. MOT16: A benchmark for multi-object tracking. *arXiv preprint arXiv:1603.00831*, 2016.
- [46] A. Milan, L. Leal-Taixé, K. Schindler, and I. Reid. Joint tracking and segmentation of multiple targets. In *CVPR*, 2015.
- [47] A. Milan, S. Roth, and K. Schindler. Continuous energy minimization for multitarget tracking. *TPAMI*, 2014.
- [48] A. Milan, S. Roth, and K. Schindler. Continuous energy minimization for multitarget tracking. *TPAMI*, 2014.
- [49] J. E. Mitchell. Branch-and-cut algorithms for combinatorial optimization problems. *Handbook of applied optimization*, pages 65–77, 2002.
- [50] P. Ochs, J. Malik, and T. Brox. Segmentation of moving objects by long term video analysis. *TPAMI*, 2014.
- [51] P. M. Pardalos and S. A. Vavasis. Quadratic programming with one negative eigenvalue is np-hard. *Journal of Global Optimization*, 1(1):15–22, 1991.
- [52] H. Pirsiavash, D. Ramanan, and C. Fowlkes. Globally-optimal greedy algorithms for tracking a variable number of objects. In *CVPR*, 2011.
- [53] H. Pirsiavash, D. Ramanan, and C. C. Fowlkes. Globally-optimal greedy algorithms for tracking a variable number of objects. In *CVPR*, 2011.
- [54] S. Ren, R. G. K. He, and J. Sun. Faster r-cnn: Towards real-time object detection with region proposal networks. *NIPS*, 2015.
- [55] S. H. Rezatofighi, A. Milan, Z. Zhang, Q. Shi, A. Dick, and I. Reid. Joint probabilistic data association revisited. In *ICCV*, 2015.
- [56] A. Sadeghian, A. Alahi, and S. Savarese. Tracking the untrackable: Learning to track multiple cues with long-term dependencies. *arXiv preprint arXiv:1701.01909*, 2017.
- [57] S. Sahni. Computationally related problems. *SIAM Journal on Computing*, 1974.
- [58] R. Sanchez-Matilla, F. Poiesi, and A. Cavallaro. Multi-target tracking with strong and weak detections. In *ECCV Workshops - Benchmarking Multi-Target Tracking*, 2016.
- [59] G. Seguin, P. Bojanowski, R. Lajugie, and I. Laptev. Instance-level video segmentation from object tracks. In *CVPR*, 2016.
- [60] Y. Song and M. Jeon. Online multiple object tracking with the hierarchically adopted gm-phd filter using motion and appearance. *ICCE*, 2016.
- [61] R. Stewart, M. Andriluka, and A. Y. Ng. End-to-end people detection in crowded scenes. In *CVPR*, 2016.
- [62] S. Tang, B. Andres, M. Andriluka, and B. Schiele. Subgraph decomposition for multi-target tracking. In *CVPR*, 2015.
- [63] S. Tang, B. Andres, M. Andriluka, and B. Schiele. Multi-person tracking by multicuts and deep matching. In *ECCV Workshops - Benchmarking Multi-Target Tracking*, 2016.
- [64] P. Weinzaepfel, J. Revaud, Z. Harchaoui, and C. Schmid. DeepFlow: Large displacement optical flow with deep matching. In *ICCV*, 2013.
- [65] A. Zamir, A. Dehghan, and M. Shah. Gmcp-tracker: Global multi-object tracking using generalized minimum clique graphs. In *ECCV*, 2012.
- [66] L. Zhang, Y. Li, and R. Nevatia. Global data association for multi-object tracking using network flows. In *CVPR*, 2008.

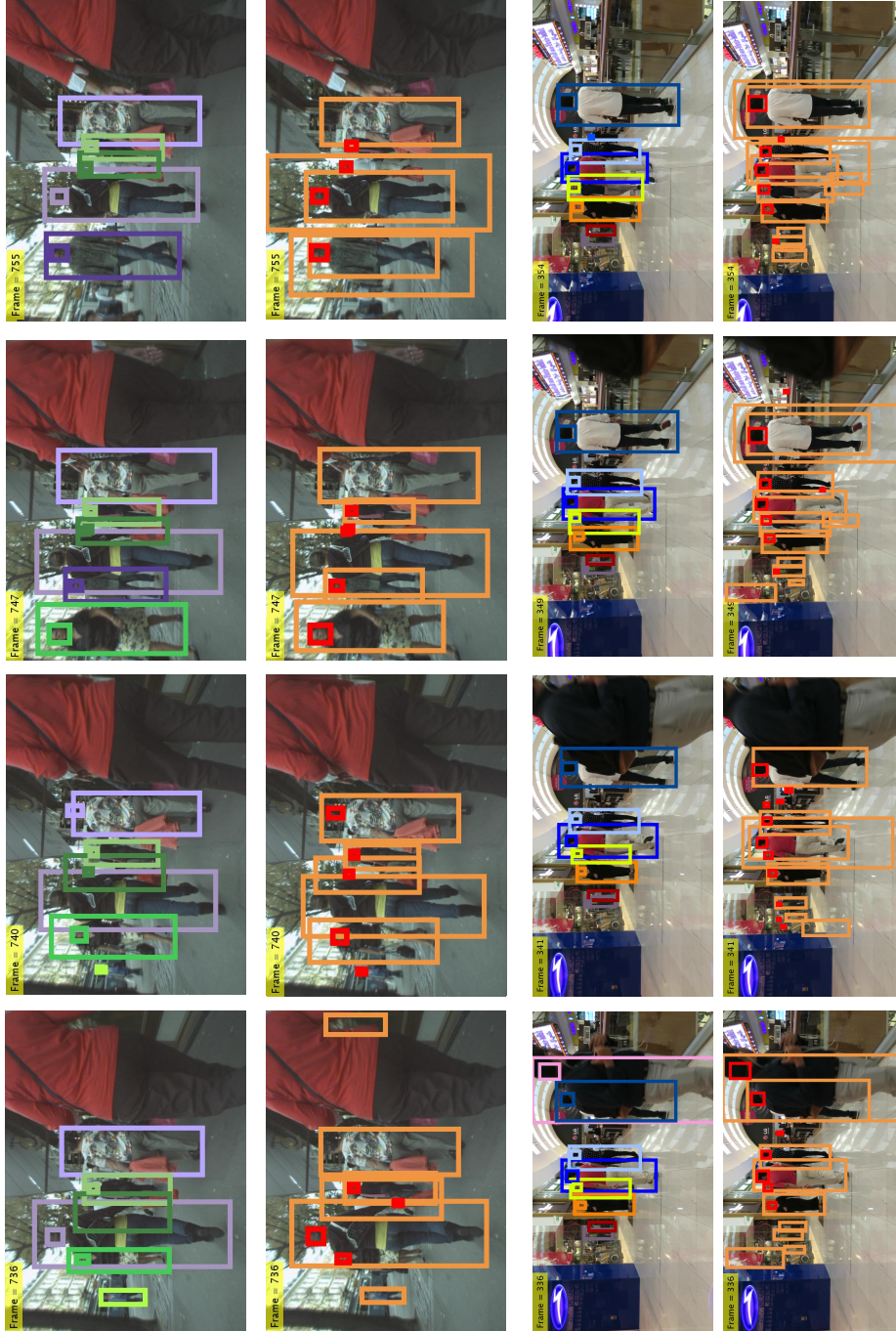


Figure 7. (First and third row) Tracking result for the sequences MOT16-05 (frames 736,740,747,755) and MOT16-11 (frames 336,341,349,354), respectively. Plotted are the full body as well as head detections. (Second and fourth row) The input detections for the corresponding frames. Drawn in yellow is the full body detection and in red the head detection.